Journal of Molecular Liquids 388 (2023) 122752

Contents lists available at ScienceDirect

Journal of Molecular Liquids

journal homepage: www.elsevier.com/locate/molliq

Electrically tunable thermoresponsive optic switch for smart window application based on dye-doped cholesteric liquid crystal

Yi-Cheng Chang [a], Sheng-Hsiung Yang [a], Victor Ya. Zyryanov [b], Wei Lee [c,*]

[a] Institute of Lighting and Energy Photonics, National Yang Ming Chiao Tung University, Guiren Dist, Tainan 711010, Taiwan
[b] Kirensky Institute of Physics, Federal Research Center "Krasnoyarsk Scientific Center," Siberian Branch of the Russian Academy of Sciences, Krasnoyarsk 660036, Russia
[c] Institute of Imaging and Biomedical Photonics, College of Photonics, National Yang Ming Chiao Tung University, Guiren Dist, Tainan 711010, Taiwan

ARTICLE INFO

Keywords:
Black dye
Liquid-crystal devices
Texture switching
Smart window
Cholesteric liquid crystal
Optical switch

ABSTRACT

We demonstrate a cholesteric liquid crystal (CLC) smart window that functions as a reversible thermo-optic switch between a transparent state at a low temperature and a low-transmission state at a higher temperature. This smart window is based on the addition of a thermoresponsive handedness-reversible chiral dopant in a mixture of a typical chiral dopant, a dichroic dye and nematic liquid crystal, yielding a thermosensitized CLC. In such a homeotropically anchored dye-doped CLC, the thickness-to-pitch ratio increases as the temperature rises, causing the device to switch from the homeotropic texture to the fingerprint texture. The absorption characteristic of the dichroic dye enables the homeotropic and fingerprint configurations in the dye-doped CLC to create two distinct transmission levels—the transparent and opaque optically stable states, respectively. Such a switching mechanism entails no additional electric power and, thus, is energy-saving. Moreover, the switching temperature at which the texture transition takes place can be actively increased by increasing voltage for the smart window. This allows the CLC device to be perfectly adaptable to the need of a user and, in turn, applicable to a wider variety of environments.

1. Introduction

Due to the impact of global warming and the energy crisis in the modern era, products that combine energy-saving and carbon-reducing technologies are gradually gaining attention. To cope with industrial decarbonization for manufacturing a green future, smart buildings have also generated a great deal of discussion. Various network and energy-saving technologies have been used in smart buildings, giving the building space itself smart features and enhancing user convenience and sustainability. Smart windows are widely adopted in smart structures. By controlling the incoming sunlight from the outdoors, a smart window not only effectively blocks the intense light and excess heat from entering the room, but regulates the indoor temperature to achieve the purpose of energy saving and carbon reduction. Moreover, light transmission can also be adjusted according to individual needs to satisfy various situations. Its market positioning has evolved from purely luxury construction products in recent years to meet the demands of mid-range office buildings and residential multi-tenant buildings. Its influence will not merely be limited to the construction and smart home industries but will gradually play a significant role as well in the automotive and new energy industries.

Smart windows are manipulated by means of different materials such as phase change substances [1], organic (PEDOT–PET) [2] and inorganic (WO_3) materials [3,4], perovskites [5] and liquid crystals (LCs) [6,7]. LC-based smart windows have been extensively studied in the past few decades. Distinct mechanisms involving electrochromic [8], thermochromic [9] and photochromic [10] principles have been suggested to control the molecular arrangement of LC so as to change the level of light transmission or color. Smart windows with electrochromic materials can change their color or transmittance by using an electrical power source [11]. An electrically controlled birefringence mode and polymer-dispersed LC (PDLC) [12] enable the regulation of the optical state of the window by changing the orientation and configuration of LC molecules in an applied electric field. Yoon's group proposed a guest–host LC which alters transmittance by switching between the fingerprint (FP) and vertical textures in a black-dye-doped cholesteric LC [13]. Furthermore, by changing the cholesteric pitch length through the modification of monomer composition in a polymer-stabilized LC (PSLC)

* Corresponding author.
E-mail address: wei.lee@nycu.edu.tw (W. Lee).

https://doi.org/10.1016/j.molliq.2023.122752
Received 30 March 2023; Received in revised form 14 July 2023; Accepted 3 August 2023
Available online 9 August 2023

[14] or addition of a redox-active chiral dopant [15] under an electric field, the reflected wavelengths and, hence, the color can be adjustable. Considering cutback in consumption of electric energy, low operation voltage should be the future direction for the development of electrochromic smart windows.

Compared with the active electrochromic technology, both the photochromic and thermochromic approaches are passive-device techniques that dictate the optical state of LC smart windows. The key to photochromic LC windows is the photoactive additive that causes reorientation of LC molecules to vary light transmission or color when exposed to light of a specific wavelength. Different types of azobenzene molecules can be employed in transparency-changing windows to convert LC reversibly from smectic-A (SmA) to cholesteric (N*) phase [16] and N* to isotropic phase [17] driven by light at particular wavelengths. The color-changing function can be realized by doping azobenzene molecules [18] or adding a photosensitive molecular motor [19]. Their revertible cis-to-trans structural transformation at a specific wavelength gives rise to the change in pitch length of the cholesteric LC (CLC), thereby changing the center wavelength of the Bragg reflection band.

The thermochromic LC smart window, on the other hand, can automatically activate light modulation in response to the dynamic ambient temperature. Guo et al. reported a novel system in which PDLC and PSLC coexist, permitting the transparent state to transfer to the scattering state through heating in accordance with the phase transition between the SmA and N* phases [20]. Incorporating a LC dimer (CB7CB) into a nematogen (5CB) under the parallel-polarizer scheme, Jiang et al. manifested a 90°-rubbed vertical-alignment cell that turns transparent at low temperature with molecular orientation normal to the substrate and opaque at high temperature as the molecules lean parallel to the substrate [21]. Thermochromic smart windows are a good candidate for energy-saving solutions in buildings. This is because the light regulation can be automatically fulfilled in compliance with the dynamic temperature change without additional energy consumption.

In this study we demonstrate a novel thermochromic dye-doped CLC smart window functioning as a thermo-optic switch between the high-transmission homeotropic (H) state at low temperatures and low-transmission FP state at higher temperatures without energy consumption. The switching temperature can be electrically adapted as desired. The combination of a thermosensitive handedness-reversible chiral molecule (TCD), which transforms from a right-handed to an achiral and then to a left-handed structure through heating [22], and a well-known left-handed chiral dopant, S811, has been successfully exploited to obtain a CLC system possessing a decreasing helical pitch at an elevated temperature. The dye-doped CLC cell with vertical anchoring in the H state appears transparent at low temperatures in that the electric field of the incident light vibrates perpendicularly to the long (or absorption) axis of the black dye molecule. In the FP configuration at high temperatures, the LC cell exhibits low transmission because the electric field of the proceeding light is partially parallel to the long axis of the dye. The texture transition temperature can be precisely tailored by supplying a constant low voltage, which empowers the LC window to better adapt to a variety of climatic or environmental conditions. In addition, one can actively switch the CLC cell from the low-transmission FP state to the high-transmission H state by an externally applied voltage.

2. Experimental

To find the temperature (T)-dependent chirality, expressed by the helical twisting power (HTP), of a specific chiral molecule in a chosen nematic host for the design of our working CLC mixture, three CLC mixtures were prepared by individually doping the right-handed chiral dopant R5011, the left-handed chiral dopant S811, and the binary chiral compound—thermosensitive chiral dopant TCD [23] plus R5011—into the host E44. The nematic LC used possesses dielectric anisotropy of 17.2 (measured at the frequency of 1 kHz and $T = 20$ ℃), birefringence

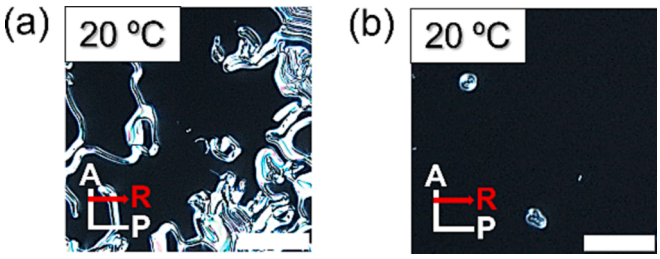

Fig. 1. POM textures (a) before and (b) after short voltage-pulse pretreatment. (Scale bar: 75 μm.)

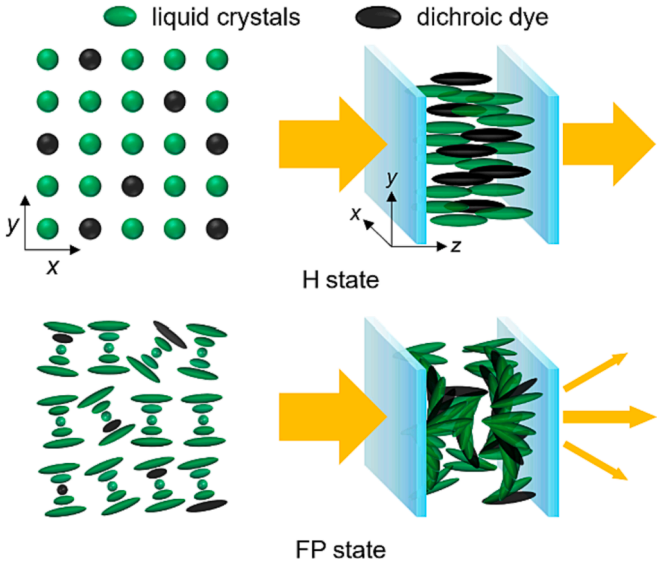

Fig. 2. The effects of dichroic dyes between the H and FP states.

of 0.242 (at the wavelength λ of 589 nm and $T = 25$ ℃), and a clearing point of ~ 93 °C. The high-HTP reagent R5011 was utilized to facilitate the investigation of the magnitude and heat-induced sign change of TCD's HTP. Three CLC samples for characterization were fabricated by filling each mixture into a commercial planar cell. Purchased from Chiptek (Miaoli, Taiwan), the empty planar cells as received have a cell gap of 6 μm and polyimide (DL-3260) coatings in antiparallel assembly. The characterization data allowed us to devise a temperature-responsive CLC for smart-window application.

The thermosensitive CLC material was concocted by adding into E44 three components: S811, TCD and the dichroic dye S428 (Mitsui Chemical Inc.) at concentrations of 2 wt%, 9.96 wt% and 0.98 wt%, respectively. The chiral dopant duo resulted in a helical pitch of ~30 μm to ensuring the normal H state at 20 °C. The dichroic dye is adopted to absorb incident light in the FP texture. The handmade LC cell comprises two electrically conductive indium–tin-oxide glass substrates whose inner surfaces were spin-coated with polyimide (AL-8395D, Daily Polymer, Kaohsiung, Taiwan) to impose vertical anchoring. The dye-doped CLC in the isotropic phase was introduced by capillary action into the vertically aligned, 180°-rubbed cell placed on top of a hotplate at about 100 °C. Made by mixing appropriate concentrations of left-handed S811 and initially right-handed TCD in the nematic host E44, the CLC is a nearly unwound system at room temperature. However, it cannot form a complete H state because of its nature of helical self-assembly (see Fig. 1(a)). The LC cell was pretreated by a short voltage pulse of 40 V_{rms} to vertically straighten the LC molecules to render an initially well-aligned H state (see Fig. 1(b)). To examine optical texture under a polarized light microscope (POM) equipped with crossed linear polarizers (Olympus BX51-P), the fabricated sample, with a cell gap of

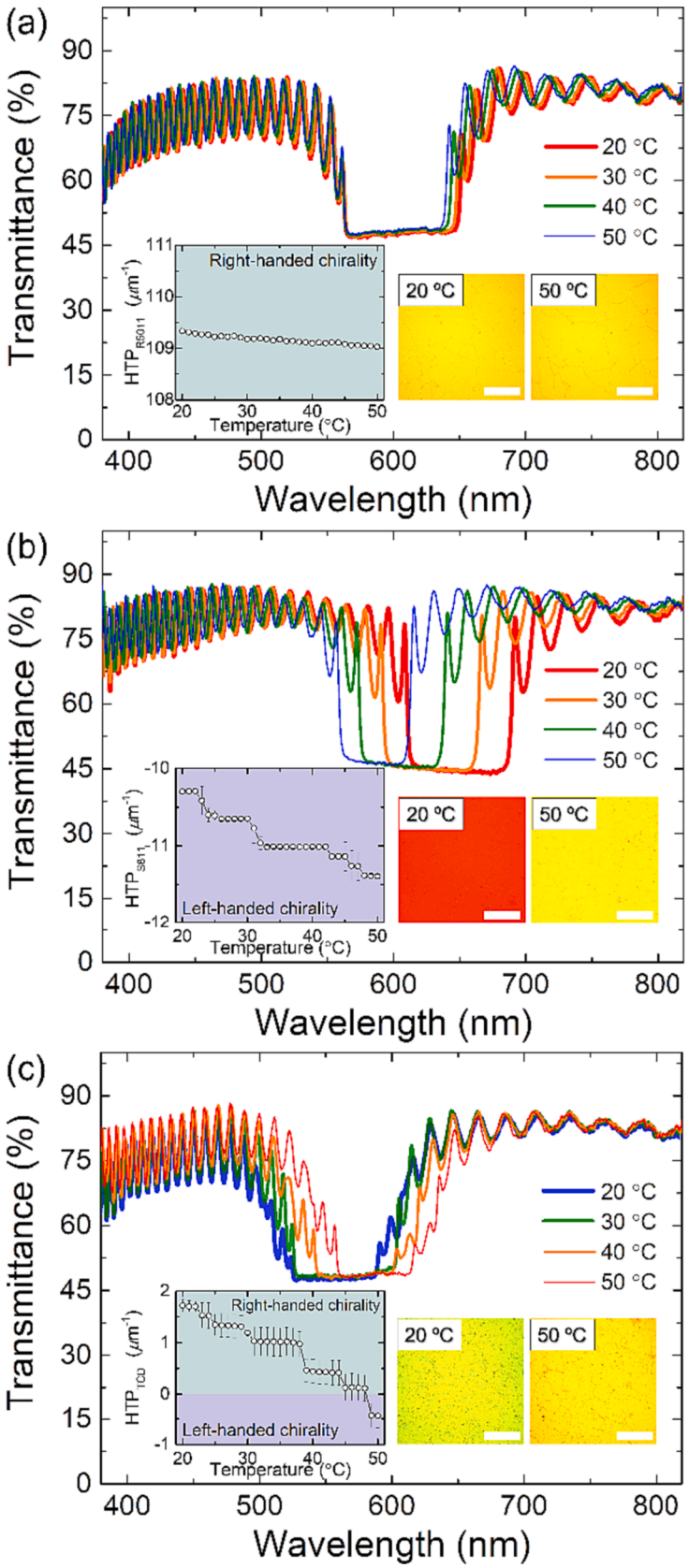

Fig. 3. Transmission spectra of E44 doped with (a) 2.49 wt% of R5011, (b) 24.50 wt% of S811, and (c) R5011 at 2.58 wt% and TCD at 10.00 wt%. Insets: T-dependent HTP and POM textures at 20 and 50 °C (scale bar: 300 μm).

9.9 μm as determined by interference, was regulated by a temperature controller (Linkam T95-PE) with an accuracy of ± 1 °C. Transmission spectra in the wavelength range between 380 and 820 nm were measured with a high-resolution, fiber-optic spectrometer (Ocean Optics HR2000+) integrated with a tungsten halogen light source (Ocean Optics HL-2000) and the haze was assessed with a haze meter (Nippon Denshoku COH-5500). AC voltage in square waveform at 1 kHz was supplied with a function generator (Tektronix AFG-3022B) in conjunction with a power amplifier (TREK Model 603).

Fig. 2 illustrates the dichroic effect of the black dye in the comparative H and FP textures. In the H state, the random polarization directions of the normally incident beam of unpolarized light are parallel to the low-absorption short axis of the dye molecule oriented by the surrounding LC molecules so that the cell is transparent. Conversely in the FP state, the polarization direction of light is partially parallel to the high-absorption axis of the dye molecule as both the LC and dye molecules twist along their lying helix via the guest–host effect, causing the cell to become nearly opaque (primarily through absorption) in the FP state.

3. Design of the thermosensitive CLC

Before determining a reasonably optimized composition for the thermosensitive CLC for demonstration of application in smart windows, we first investigated the *T*-dependent HTP of the chiral molecules S811 and TCD separately in the nematic host E44 which exhibits the ordinary refractive index $n_o = 1.5484$ and extraordinary refractive index $n_e = 1.7904$ at $\lambda = 589$ nm and $T = 25$ °C. The helical pitch p of a CLC in the Grandjean planar state is given by the equation:

$$p = \lambda_c / \langle n \rangle, \tag{1}$$

where λ_c is the central wavelength of the Bragg reflection band and $\langle n \rangle$ is the arithmetic average of n_e and n_o. On the other hand, the pitch length of a CLC made of a minute amount of optically active material in a nematic host can also be expressed by the following equation:

$$p = \frac{1}{|\mathrm{HTP} \cdot c|}, \tag{2}$$

where HTP, typically in μm^{-1}, depends on the material properties of the chiral molecules, and c is the weight- percent concentration of the chiral dopant. The combination of Eqs. (1) and (2) allows one to obtain, in the dilute limit, or approximately estimate the HTP value, whose sign is positive for right-handed and negative for left-handed chirality.

As a reference, Fig. 3(a) shows the transmission spectra of E44 doped with 2.49 wt% of right-handed R5011 at four representative temperatures. The central reflection wavelength and the texture remained nearly unchanged at temperatures spanning from 20 to 50 °C. With *T*-dependent dispersions taken into account by means of a refractometer (ATAGO DR-M4) and the extended Cauchy equations to deduce the refractive indices, the HTP of R5011 in E44 was calculated to be ca. 109.2 μm^{-1} in the temperature range of 30 °C (left inset, Fig. 3(a)). Fig. 3 (b) reveals the spectral profiles of E44 doped with S811 at 24.5 wt%, presenting the blueshift in λ_c from 652.7 to 588.6 nm as *T* increased from 20 to 50 °C. The POM images display the substantial color change of selective reflection at two limiting temperatures. According to Eqs. (1) and (2), HTP of S811 in E44 was approximated − 10.3 μm^{-1} at 20 °C and − 11.4 μm^{-1} at 50 °C.

In the case of a dilute CLC solution containing a low concentration of a binary chiral solute, the pitch length can be written as [24]

$$p = \frac{1}{|\mathrm{HTP}_1 \cdot c_1 + \mathrm{HTP}_2 \cdot c_2|} \tag{3}$$

by ignoring the intermolecular force between two chiral compounds. For the binary chiral dopant constituted by 2.58- wt% R5011 and 10.00- wt % TCD in E44, *T*-varying HTP of TCD, HTP_2, can be calculated by plugging Eq. (1) into Eq. (3) with given HTP of R5011, HTP_1 (Fig. 3(a)). The transmission spectra as shown in Fig. 3(c) indicate that λ_c redshifted from 558.3 to 618.2 nm as *T* rose from 20 to 50 °C. The reflection POM images readily show the thermochromic phenomenon. Accordingly, the HTP value changes from positive (+1.7 μm^{-1}) at 20 °C to negative (−0.4 μm^{-1}) at 50 °C (Fig. 3(c)) and −2.25 μm^{-1} at 70 °C (not shown in the figure), which means that the chirality of TCD will transfer from right-handedness (to achirality and) to left-handedness through heating.

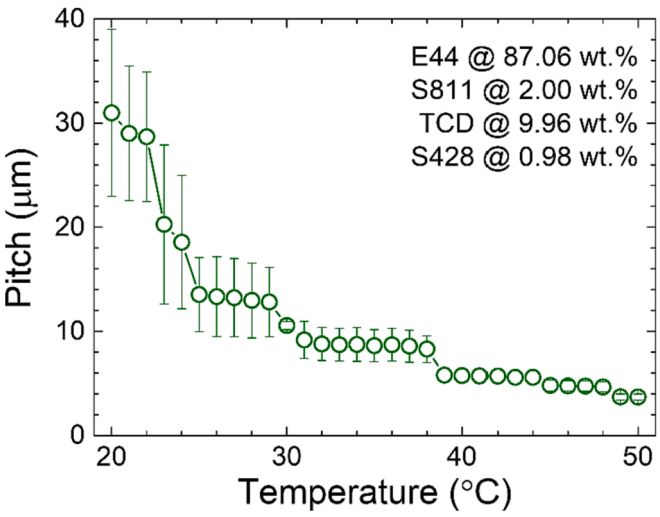

Fig. 4. Temperature-dependent pitch of the dye-doped CLC system.

After grasping the *T*-dependent helical twisting behaviors of both S811 and TCD in E44, we calculated to seek an appropriate concentration of each chiral dopant to prepare the thermosensitive CLC system, designating 2.00 wt% of S811 and 9.96 wt% of TCD for this work. The black dye S428 at a concentration of 0.98 wt% was also chosen to generate contrasted levels of transmission in two LC textures. By using a left-handed agent (S811) together with an initially chirality-counteracting dopant (TCD), the torque becomes so weak that the LC molecules are unable to take the twist at relatively low temperatures. However, the net left-handed chirality of the system grows as *T* rises, prompting the pitch length to shrink at higher temperatures. Fig. 4 delineates the calculate *d*/*p* function varying with *T* between 20 and 50 °C in accordance with Eq. (3).

4. Results and discussion

The working principles and switching mechanisms are schematically shown in Fig. 5 for the devised CLC cell featuring *T*-dependent *d*/*p* ratio. Fig. 5(a) shows two passive control techniques. One is that the LC cell, in response to the temperature variation, reversibly switches between the transparent (H) and opaque (FP) states without voltage ($V = 0$). The concentrations of S811 and TCD are crucial to decisively determine the switching temperature (at which the state changes) at null applied voltage. The other signifies that the switching temperature can be desirably raised by voltage, manipulating the onset of state transition at a higher ambient temperature. In addition, Fig. 5(b) shows the active control mechanism underlying the *V*-regulated state selection from the opaque FP to transparent H texture at a given temperature by virtue of the dielectric effect in LC.

Fig. 6 shows the transmission POM textures of a thermosensitive CLC system in a vertically aligned cell at various temperatures, with the transmission axis of the polarizer (P) in the same direction as the alignment of the LC cell. At 20 °C, the CLC is in the H state because the strength of helical self-assembly of the LC is too weak to compete with the vertical anchoring force. As the temperature rises, the winding of the

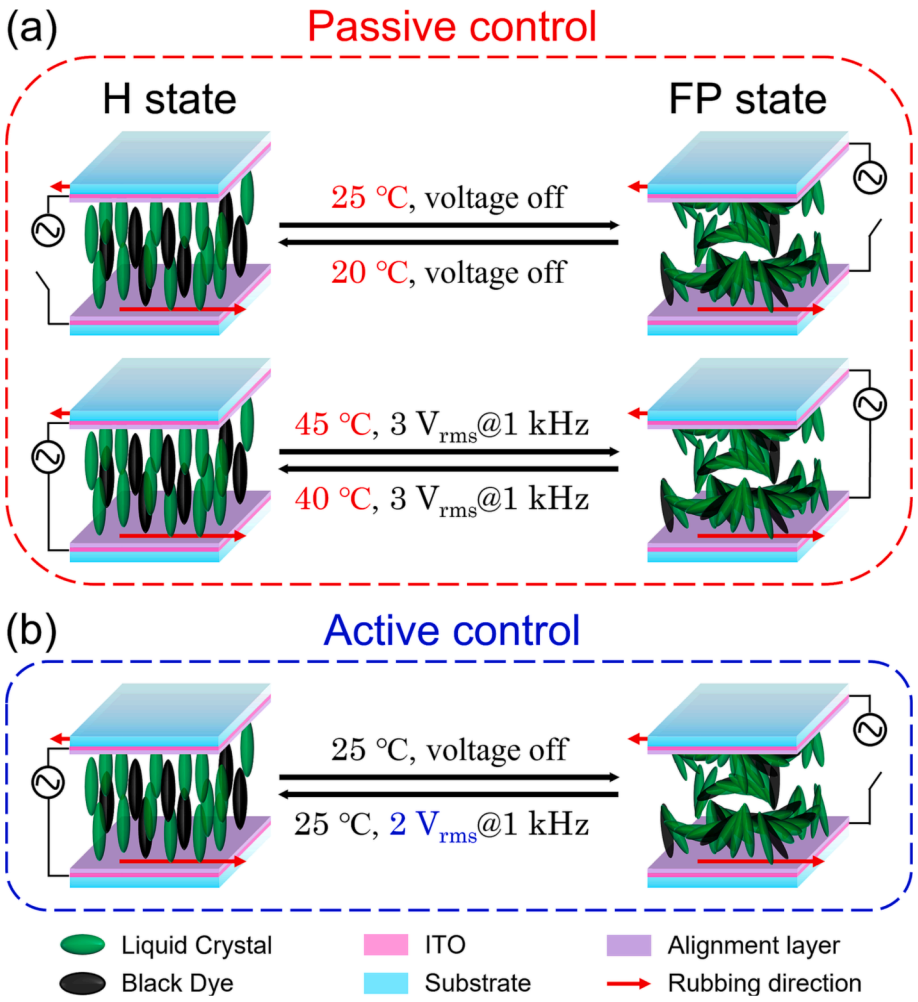

Fig. 5. Activation of texture transition: (a) passive control by responding to the temperature change with or without AC voltage; (b) active control by applied AC voltage at a fixed temperature.

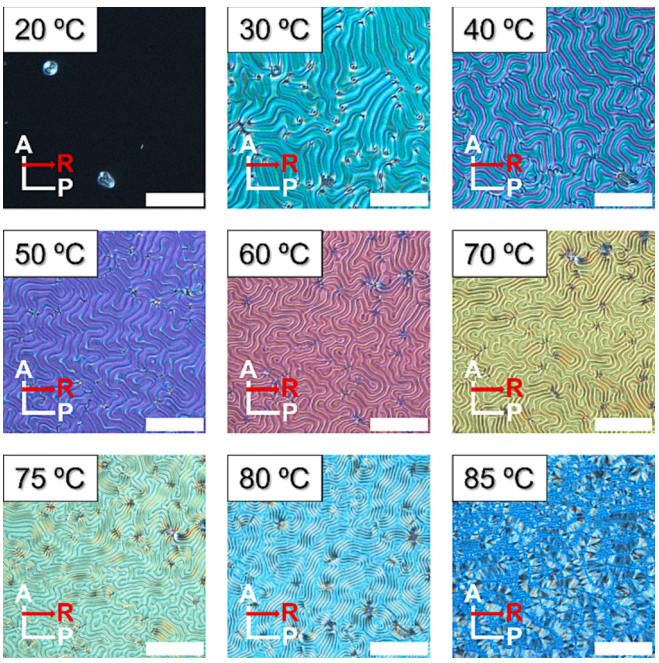

Fig. 6. POM textures at various temperatures at 0 V. (Scale bar: 75 μm.)

CLC system becomes stronger, unambiguously showing FP texture from 30 °C to 80 °C. The optical texture at even higher temperatures reveals that the pitch of the fingerprints shrinks gradually with increasing temperature and enters the focal conic state at about 85 °C.

Transmission spectrometry offers a direct and useful means to characterize the device performance of thermo-optic response. Without using a polarizer in the spectral measurement, average transmittance is defined as the transmission data averaged in the wavelength range from 450 to 650 nm. The heating or cooling rate was controlled at 1 °C per minute. When T increased from 20 to 25 °C (region I), transmittance decreased from 72.8 to 18.9% and the haze increased from 1.1 to 27.3% at zero voltage (Fig. 7(a)). We inspected POM images taken in the transmission mode with crossed polarizers to better understand the decrease in transmission. At 20 °C, the LC cell exhibited H texture and most of incident light was transmitted through the cell because the LC and dye molecules in this state are oriented vertically. As T rose to 23 °C, the POM image showed a FP texture, connoting that the helical torque in the self-assembled LC bulk overcame the vertical surface anchoring. In thus-formed FP configuration, the LC and dye molecules twisted along the helical lying axis parallel to the substrate plane. As a result, the dichroic dye significantly absorbed unpolarized light with an arbitrary polarization. When T increased further (region II), the pitch dropped due to the stronger chirality in the CLC at higher T. Apart from absorption, the enhanced haze suggested nontrivial light scattering in the FP state. Likewise, Fig. 7(b) shows average transmittance and haze in the temperature range from 20 to 50 °C at 3 V$_{rms}$. The general behaviors are

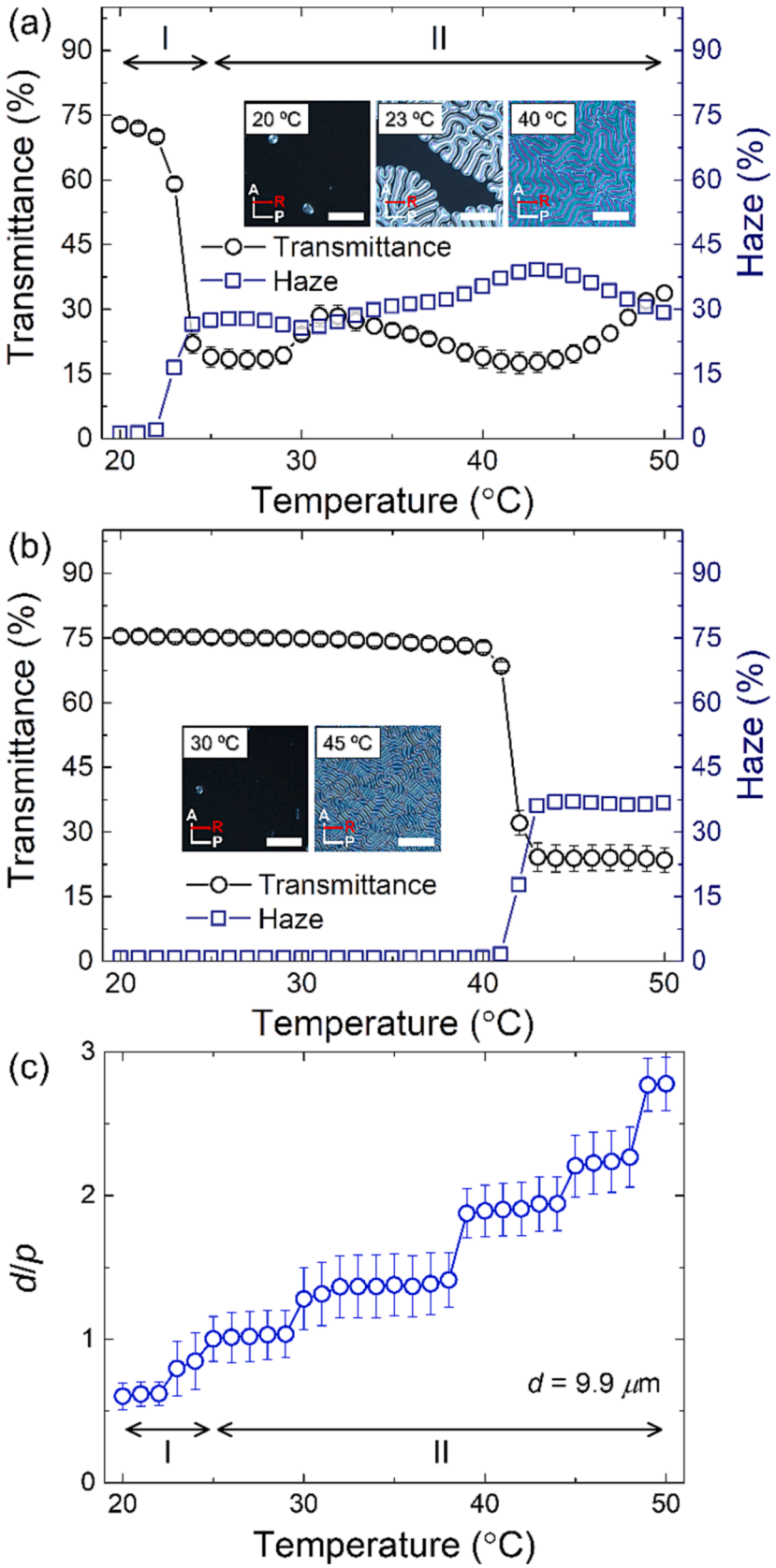

Fig. 7. Temperature-dependent average transmittance and haze at (a) 0 V and (b) 3 V_{rms}. (c) Thickness-to-pitch ratio as a function of the temperature at 0 V. Insets in (a) and (b): POM textures at various temperature. (Scale bar in each inset: 75 μm.).

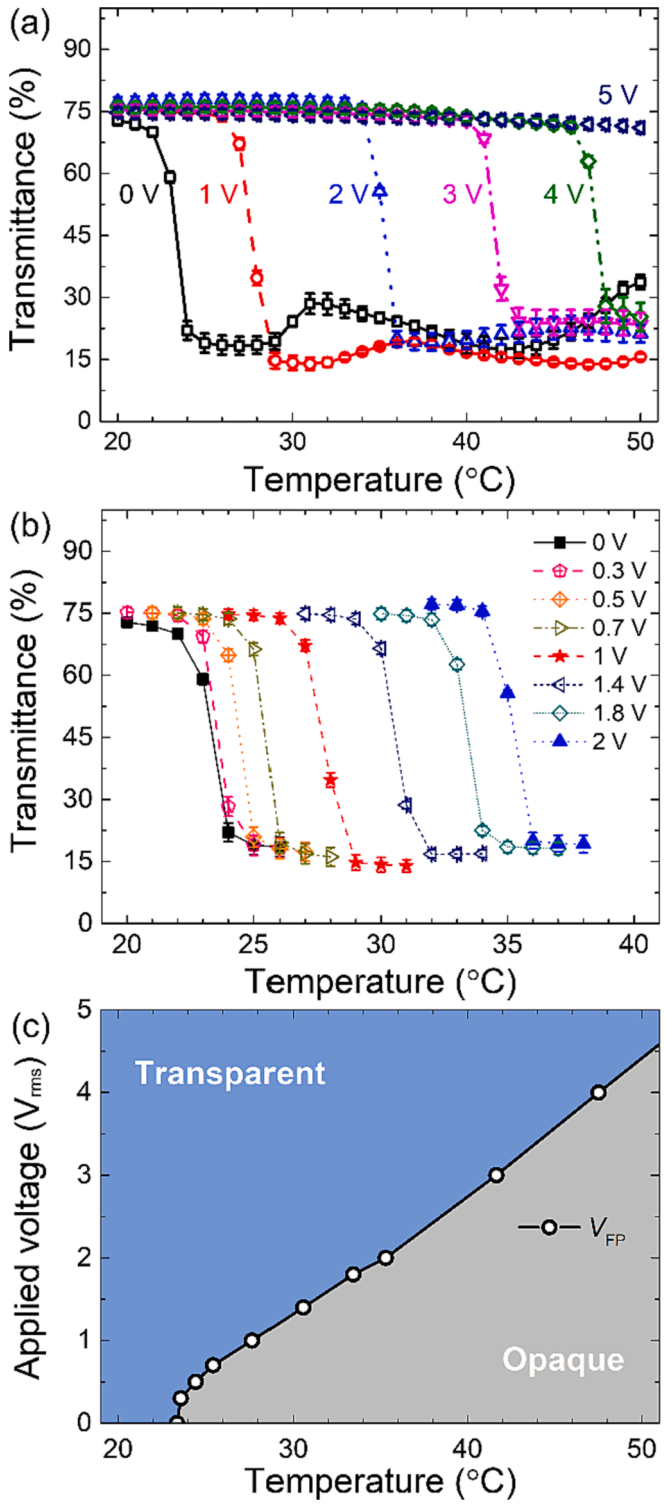

Fig. 8. Average transmittance vs. temperature at various applied voltages in the ranges (a) from 0 to 5 V_{rms} and (b) between 0 and 2 V_{rms} for demonstration of finer control of the switching temperature. (c) Temperature-dependent applied voltage to impel the cell to the opaque and transparent regimes.

similar to the results at null voltage (Fig. 7(a)) except that the switching temperature to actuate the transition between the high- and low-transmission states gets higher. One can see from Fig. 7(a) and (b) that transmission and texture of the proposed CLC cell converted at 23 °C at 0 V and 42 °C at 3 V_{rms}.

Also to find the relationship between the switching temperature and

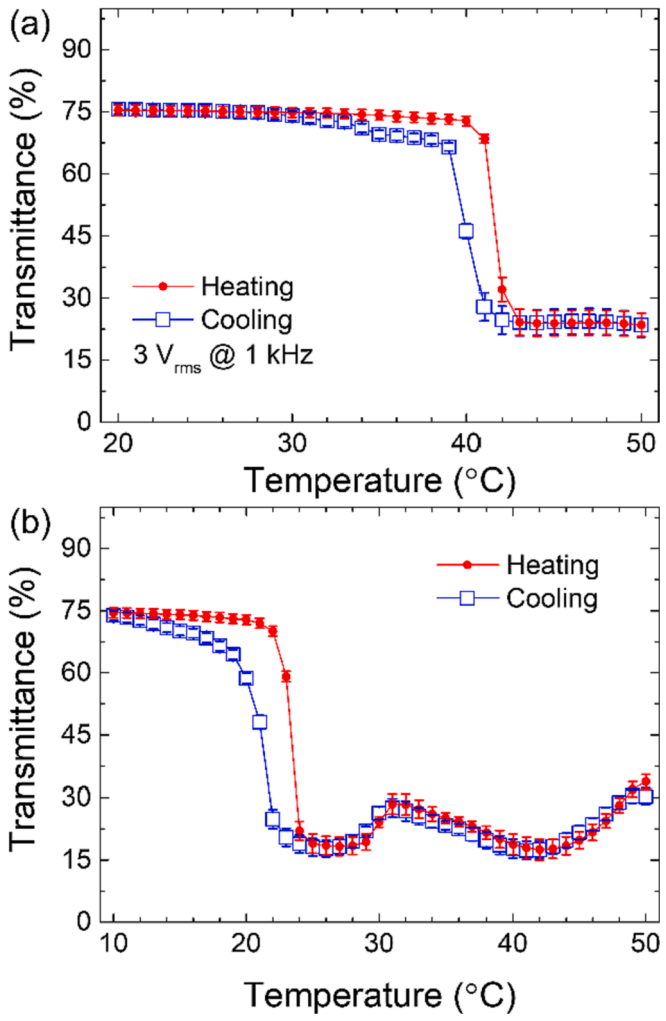

Fig. 9. Reversibility examination of the cell (a) at 3 V_{rms} and (b) without applied voltage.

d/p ratio, we calculated the *T*-dependent *d/p* ratio of the 9.9-μm cell and plotted Fig. 7(c) accordingly. With the specifically designed homeotropic anchoring cell, the texture of the dye-doped CLC transferred from the H to FP state as the helical pitch shortened with increasing temperature. The H-to-FP or FP-to-H transition is ruled by the ratio of the cell thickness to the pitch length of the CLC. In comparison with Fig. 7(a), Fig. 7(c) implies that the dye-doped CLC mainly remained homeotropic as $d/p < 0.5$ because of the vertical-alignment surface boundaries but transformed into a lying-helix texture (i.e., FP texture) at $d/p > 0.5$ in the operation mode of no power consumption (i.e., $V = 0$).

We then applied various AC voltages at frequency of 1 kHz to investigate the effect of persistent voltage on passive temperature regulation. Fig. 8(a) depicts *T*-dependent average transmittance of the LC cell at several voltages between 0 and 5 V_{rms} by one-volt intervals. It is clear from Fig. 8(a) that the switching temperature for texture transition rises as *V* increases. Since E44 has positive dielectric anisotropy, applied voltage causes an electric torque to orient the LC perpendicularly to the substrate. Because such applied voltage tends to stretch the helical pitch or unwind the twist and, in turn, reduce the *d/p* ratio, the transition from the H to FP configuration will occur at a higher temperature where and beyond which the helical twisting force of the chiral LC is greater than the sum of the vertical anchoring force and the electric field force. The absorption characteristic of the dichroic dye varies in the two dissimilar textures. Both the FP and H textures in the dye-doped CLC can be exploited to create the opaque and transparent states,

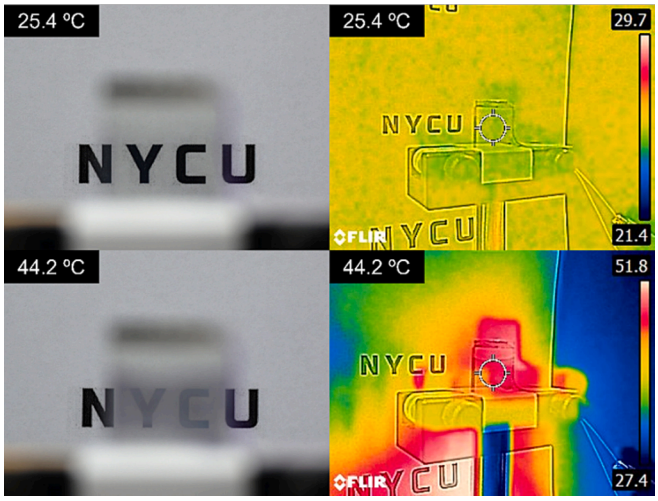

Fig. 10. Demonstration of the thermally adaptive smart control of the transmission of the CLC window at varying temperatures monitored by an infrared camera. The emblem "NYCU" is 10 cm in distance behind the CLC cell at 3 V_{rms}.

respectively. Fig. 8(b) presents average transmittance within a smaller voltage range of $0 \leq V \leq 2$ V_{rms} for observing the voltage tuning of the switching temperature more closely. Plotted using data retrieved from both Fig. 8(a) and (b), Fig. 8(c) shows how the voltage and ambient temperature interplay to designate the optical state. The zone boundary as displayed in the figure is specified by the V_{FP} curve, where the switching voltage V_{FP} at a given T corresponds to 45% in transmittance. As disclosed in Fig. 8(c), the switching temperature shifted to ~28 °C at 1 V_{rms} compared with 24 °C at 0 V. The switching temperatures were 36, 42 and 48 °C at 2, 3 and 4 V_{rms}, respectively. In the extreme case at $V = 5$ V_{rms}, the dye-doped CLC cell retained its high transparency up to 53 °C (not shown in the figure). It is confirmed that by applied voltage one can finely control the switching temperature at which the system enters the mixed state.

Manifesting the reversibility of the switching direction, Fig. 9(a) representatively reveals a tendency at 3 V_{rms} as also detailed in Fig. 9(b) at 0 V. The CLC took inertial characteristics from the preceding texture, leading to the obstinate hysteresis between the heating and cooling curves. Such phenomenological hysteresis became expectedly less pronounced under a sustaining voltage ($V \neq 0$).

Light transmission of the switchable CLC cell can be managed by both the thermal and electrical controls. This feature offers a different way of regulating the transparency in different applications. Referring to Fig. 8(c), one can anticipate switchability in transmittance by applied voltage at a given temperature above a threshold, which is 23.5 °C in this study. This voltage manipulates the dye-doped CLC bulk to selectively take either H or FP configuration. The cell's transparency is remarkably lowered when the LC exhibits the FP state, as opposed to the high-transmittance H state compelled by a voltage beyond the T-dependent switching voltage V_{FP} ($V > V_{FP}$). Following Fig. 9(a), Fig. 10 shows the photos of four characters (as an initialism) behind a CLC cell driven by 3 V_{rms} at two dissimilar temperatures of 25 and 44 °C, yielding the high-transmission H and low-transmission FP states in the dye-doped CLC, respectively. The right panels display the associated thermographs acquired with an infrared camera (FLIR ThermaCam E4).

5. Conclusion

In summary, a guest–host CLC confined in a vertically aligned cell was fabricated by mixing two chiral compounds, TCD and S811, to enable its electrically tunable thermo- responsiveness. At null voltage, the dye-doped LC preserved its H state as the ratio $d/p < 0.5$ whereas it exhibited the FP texture otherwise. Because of absorption anisotropy in the dichroic guest, the H and FP textures bring about the transparent and low-transmission states, respectively. The state transition or two-level transmission transfer in the CLC as an optic switch for the extended application in smart glass is passively governed by ambient temperature. A surrounding temperature below (beyond) the characteristic switching temperature for texture transition gives the optically stable H (FP) state. In addition to the T-controlled texture or state transition, we demonstrated that the switching temperature can be actively increased by increasing an externally applied voltage across the cell thickness. The switching is cyclically reversible between the two optical states. This work intended to provide proof of concept. A lower threshold temperature to permit the choice of the low-transmission FP texture is possible, making the smart window more user-friendly.

CRediT authorship contribution statement

Yi-Cheng Chang: Conceptualization, Data curation, Formal analysis, Investigation, Methodology, Writing – original draft. **Sheng-Hsiung Yang:** Data curation, Project administration, Supervision. **Victor Ya. Zyryanov:** Conceptualization, Validation. **Wei Lee:** Conceptualization, Data curation, Funding acquisition, Project administration, Resources, Supervision, Validation, Writing – review & editing.

Declaration of Competing Interest

The authors declare that they have no known competing financial interests or personal relationships that could have appeared to influence the work reported in this paper.

Data availability

Data will be made available on request.

Acknowledgment

This work was financially supported by National Science and Technology Council, Taiwan (NSTC), under Grant Nos. 110-2112-M-A49-023 and 111-2112-M-A49-033.

References

[1] R.N. Wijesena, N.D. Tissera, V. Rathnayaka, H. Rajapakse, R.M. de Silva, K.N. de Silva, Shape-stabilization of polyethylene glycol phase change materials with chitin nanofibers for applications in "smart" windows, Carbohydr. Polym. 237 (2020), 116132.
[2] K. Wang, H. Wu, Y. Meng, Y. Zhang, Z. Wei, Integrated energy storage and electrochromic function in one flexible device: an energy storage smart window, Energ. Environ. Sci. 5 (2012) 8384–8389.
[3] Z. Xie, X. Jin, G. Chen, J. Xu, D. Chen, G. Shen, Integrated smart electrochromic windows for energy saving and storage applications, Chem. Commun. 50 (2014) 608–610.
[4] P. Yang, P. Sun, Z. Chai, L. Huang, X. Cai, S. Tan, J. Song, W. Mai, Large-scale fabrication of pseudocapacitive glass windows that combine electrochromism and energy storage, Angew. Chem. 126 (2014) 12129–12133.
[5] Y. Liu, J. Wang, F. Wang, Z. Cheng, Y. Fang, Q. Chang, J. Zhu, L. Wang, J. Wang, W. Huang, Full-frame and high-contrast smart windows from halide-exchanged perovskites, Nat. Commun. 12 (2021) 1–8.
[6] W.J. Yoon, Y.J. Choi, S.I. Lim, J. Koo, S. Yang, D. Jung, S.W. Kang, K.U. Jeong, A single-step dual stabilization of smart window by the formation of liquid crystal physical gels and the construction of liquid crystal chambers, Adv. Funct. Mater. 30 (2020) 1906780.
[7] M. Sheng, J. Li, X. Jiang, C. Wang, J. Li, L. Zhang, S. Fu, Biomimetic solid–liquid transition structural dye-doped liquid crystal/phase-change-material microcapsules designed for wearable bistable electrochromic fabric, ACS Appl. Mater. Interfaces 13 (2021) 33282–33290.
[8] M. Wang, X. Xing, I.F. Perepichka, Y. Shi, D. Zhou, P. Wu, H. Meng, Electrochromic smart windows can achieve an absolute private state through thermochromically engineered electrolyte, Adv. Energy Mater. 9 (2019) 1900433.
[9] M. Aburas, V. Soebarto, T. Williamson, R. Liang, H. Ebendorff-Heidepriem, Y. Wu, Thermochromic smart window technologies for building application: A review, Appl. Energy 255 (2019).

[10] D. Cao, C. Xu, W. Lu, C. Qin, S. Cheng, Sunlight-driven photo-thermochromic smart windows, Sol. RRL 2 (2018) 1700219.
[11] Y. Ke, J. Chen, G. Lin, S. Wang, Y. Zhou, J. Yin, P.S. Lee, Y.i. Long, Smart windows: electro-, thermo-, mechano-, photochromics, and beyond, Adv. Energy Mater. 9 (39) (2019) 1902066.
[12] C. Li, M. Chen, L. Zhang, W. Shen, X. Liang, X. Wang, H. Yang, An electrically light-transmittance-switchable film with a low driving voltage based on liquid crystal/polymer composites, Liq. Cryst. 47 (2020) 106–113.
[13] S.-W. Oh, S.-M. Ji, C.-H. Han, T.-H. Yoon, A cholesteric liquid crystal smart window with a low operating voltage, Dyes Pigm. 197 (2022), 109843.
[14] B.P. Radka, B.E. King, M.E. McConney, T.J. White, Electrically induced splitting of the selective reflection in polymer stabilized cholesteric liquid crystals, Adv. Opt. Mater. 8 (2020) 2000914.
[15] S. Tokunaga, Y. Itoh, H. Tanaka, F. Araoka, T. Aida, Redox-responsive chiral dopant for quick electrochemical color modulation of cholesteric liquid crystal, J. Am. Chem. Soc. 140 (2018) 10946–10949.
[16] Z.-Y. Kuang, Y. Deng, J. Hu, L. Tao, P. Wang, J. Chen, H.-L. Xie, Responsive smart windows enabled by the azobenzene copolymer brush with photothermal effect, ACS Appl. Mater. Interfaces 11 (40) (2019) 37026–37034.
[17] S.-W. Oh, S.-M. Nam, S.-H. Kim, T.-H. Yoon, W.S. Kim, Self-regulation of infrared using a liquid crystal mixture doped with push–pull azobenzene for energy-saving smart windows, ACS Appl. Mater. Interfaces 13 (4) (2021) 5028–5033.
[18] H. Wang, H.K. Bisoyi, A.M. Urbas, T.J. Bunning, Q. Li, Reversible circularly polarized reflection in a self-organized helical superstructure enabled by a visible-light-driven axially chiral molecular switch, J. Am. Chem. Soc. 141 (20) (2019) 8078–8082.
[19] Q. Wang, L.i. Yu, J. Sun, Y.u. Guan, Z. Zhou, Y. Shin, H. Yang, J. West, D.-K. Yang, Sunlight-driven self-organized helical superstructure chromotropic device, Adv. Opt. Mater. 8 (24) (2020) 2001207.
[20] S.-M. Guo, X. Liang, C.-H. Zhang, M. Chen, C. Shen, L.-Y. Zhang, X. Yuan, B.-F. He, H. Yang, Preparation of a thermally light-transmittance-controllable film from a coexistent system of polymer-dispersed and polymer-stabilized liquid crystals, ACS Appl. Mater. Interfaces 9 (3) (2017) 2942–2947.
[21] Y. Jiang, Y. Zhou, M. Wang, D.-K. Yang, Smart Thermally Switchable Liquid Crystal Window, Adv. Photonics Res. 2 (2021) 2000156.
[22] Y.-C. Hsiao, Z.-H. Yang, D. Shen, W. Lee, Red, green, and blue reflections enabled in an electrically tunable helical superstructure, Adv. Opt. Mater. 6 (2018) 1701128.
[23] G. Heppke, D. Lötzsch, F. Oestreicher, Esters of (S)-1, 2-propanediol and (R, R)-2, 3-butanediol—chiral compounds inducing cholesteric phases with a helix inversion, Z. Naturforsch. A 42 (1987) 279–283.
[24] Y.-J. Liu, P.-C. Wu, W. Lee, Spectral variations in selective reflection in cholesteric liquid crystals containing opposite-handed chiral dopants, Mol. Cryst. Liq. Cryst. 596 (2014) 37–44.